Article

Photocatalytic Degradation of Ciprofloxacin by UV Light Using N-Doped TiO$_2$ in Suspension and Coated Forms

Sarah A. Abdulrahman [1], Zainab Y. Shnain [1,*], Salah S. Ibrahim [1,*] and Hasan Sh. Majdi [2]

[1] Chemical Engineering Department, Faculty of Engineering, University of Technology-Iraq, Baghdad 10066, Iraq

[2] Department of Chemical Engineering and Petroleum Industries, Al-Mustaqbal University College, Babylon 51001, Iraq

* Correspondence: zainab.y.shnain@uotechnology.edu.iq (Z.Y.S.); salah.s.ibrahim@uotechnology.edu.iq (S.S.I.)

Abstract: The presence of organic compounds such as ciprofloxacin in untreated pharmaceutical wastewater often poses a serious health risk to human and aquatic life when discharged into water bodies. One of the most effective means of removing ciprofloxacin from wastewater is photocatalytic degradation. However, the synthesis of an effective photocatalyst that can degrade the organic pollutant in the wastewater is often a challenge. Hence, this study focuses on the synthesis and application of nitrogen-doped TiO$_2$ (N-TiO$_2$) in suspension and coated forms for the photocatalytic degradation of ciprofloxacin in wastewater by applying UV-light irradiation. The nitrogen-doped TiO$_2$ photocatalyst was prepared by a co-precipitation process and characterized using energy-dispersive X-ray spectroscopy, scanning electron microscopy, and Fourier-transform infrared spectroscopy. The effects of the initial concentration of the ciprofloxacin (6, 12, 18, or 30 ppm), pH (3, 5, 7, or 9), and flow rate (0.4, 0.8, 0.95, or 1.5 L/min) on the degradation of the ciprofloxacin over the N-TiO$_2$ were investigated. The results showed that the removal efficiency of ciprofloxacin was enhanced by increasing the initial ciprofloxacin concentration, while it was decreased with the increase in the feed flow rate. The best operating conditions were obtained using an initial ciprofloxacin concentration of 30 ppm, pH of 5, and feed flow rate of 0.4 L/min. Under these operating conditions, removal efficiencies of 87.87% and 93.6% were obtained for net TiO$_2$ and N-TiO$_2$ of 5 wt% in suspension form, respectively, while 94.5% ciprofloxacin removal efficiency was obtained using coated 5 wt% N-TiO$_2$ after 2 h of photocatalytic degradation. Based on the response surface optimization strategy, a quadratic model was suggested to obtain mathematical expressions to predict the ciprofloxacin removal efficiency under various studied operational parameters.

Keywords: photocatalysis; ciprofloxacin; titanium dioxide TiO$_2$; N-doped TiO$_2$

1. Introduction

Pollution and industrial waste endanger water resources, damaging and destroying the world's ecosystems. One of the most pressing environmental problems in recent decades is the damage caused by persistent organic pollutants (POPs) [1]. Among the most dangerous contaminants of wastewater are pharmaceutical products, of which antibiotics are the most dangerous organic compounds due to their wide range of use as a class of drugs in both human and veterinary medicine [2]. These compounds are capable of causing serious negative effects in organisms that are improperly exposed to them, due to their ability to interfere with hormones and to cause abnormalities and cancers [3]. The discharge of these pharmaceutically active compounds (PhACs) into water sources is a major public health concern [4].

Antibiotics are often found in high concentrations in water bodies and are only partially eliminated by standard water-treatment methods [5,6]. Ciprofloxacin (CIP) is a second-generation fluoroquinolone. It has been widely used to stop or treat infectious

diseases in humans and animals [7]. CIP concentrations between μg and mg per liter, when found in water bodies, have a negative impact on the formation and functioning of natural microbial communities, including antagonistic competition and metabolites that give rise to antibiotic resistance genes, bacterial resistance, and potential negative effects on human health [8,9].

Traditional physical techniques have been used in the past to remove various contaminants from polluted water, including adsorption on activated carbon and polymer compounds [10–12], ultrafiltration, reverse osmosis, coagulation using chemical agents, ion exchange on synthetic absorbent resins, and catalytic reductase [13], while there have been many attempts to establish methods for removing antibiotics from water. These methods include absorption [8,14], membrane bioreactors [5,15], ozone [12], ultrasonic radiation, and solid polymers [16,17]. Studies have revealed that these various approaches appear promising and are effective in eliminating CIP from wastewater. Due to its effectiveness in eliminating various environmental pollutants, titanium dioxide (TiO_2) has been used as a catalyst for the reaction in the photocatalytic process [18].

Semiconducting photocatalysis has been demonstrated to be an effective green method for eliminating several of the above pollutants. Researchers are motivated to create visible light-active photocatalysts, since UV light's negligible contribution to the solar spectrum incident on Earth (less than 5%) is a crucial consideration [19]. The most extensively used photocatalysts for numerous pollutants are made of TiO_2 and other compounds that contain titanium [20].

TiO_2 catalysts are characterized by high activity, impermeability to poisons, low cost, stability in prolonged use at elevated temperatures, and physical and chemical stability under many conditions [21,22]. On the other hand, TiO_2 creates a hole because it exclusively absorbs UV wavelengths and has a large bandgap (3.2 eV), along with a high hole for photogeneration (h^+)/electron pair recombination rate (e) [21] to enhance conformation and broaden the visible light absorption spectra [23]. The catalyst-loading process with nonmetal and metallic doping is preferred. Recently, many studies have focused on various modifications of TiO_2 to improve its activity under UV irradiation or to reduce the bandgap energy so that visible light can be used [24]. Rahman et al. provided an overview of several modification techniques that can improve the activity of TiO_2 under visible light [19,25]. The loading process can change the bandgap in different ways, reducing the conduction area and increasing the valence area of the cofactor; Thus, the cofactor responds to visible light [26]. Among these dopants are nonmetals (e.g., N, S, C, F, Cl), metals (e.g., Fe, V, Cr, Mn, Co, Ni, Cu, Pt, etc.), and others [27]. It is known that the only way to activate TiO_2 is to use photon energy greater than the bandgap energy [5]. As a result, TiO_2 has been prepared using different synthesis techniques to bridge the energy gap and discover suitable features that enable greater photocatalytic activity [4,6–8]. The use of complex phases that are sometimes difficult to regulate during the synthesis process—because they are relatively expensive or require long preparation times—can be incorporated into synthesis methods such as spray pyrolysis, the sol–gel method, and others [27]. It is desirable to find direct and environmentally acceptable technologies that produce N-doped TiO_2 at lower temperatures.

The preparation of semiconductors by co-deposition is simple and inexpensive [23,25,26]. The synthesis of Cu/N-doped TiO_2 has been reported. Hoffman et al. [27] used a template-free homogeneous co-sedimentation approach followed by the traditional method. Moreover, various researchers have investigated the removal of ciprofloxacin from wastewater using PCP. Gad-Allah et al. [28] worked on the removal of CIP using a 1000 mg/L TiO_2 photocatalyst under sunlight. Their findings revealed that 94% of CIP was removed using a concentration of 50 ppm after 120 min. Durán-Álvarez et al. [29] found that the removal of CIP after loading the TiO_2 catalyst with metal particles (i.e., Au, Ag, and Cu) was more efficient than that of the pristine TiO_2. The CIP removal was 63% after 180 min when its concentration was 30 ppm. Zheng et al. [30] found that 94% of CIP was removed after optimizing the catalyst with the PCP procedure and using conditions such as 0.35 g/L

porous graphitized mesoporous carbon TiO_2 (GMC-TiO_2). Malakootian et al. [31] studied the removal of CIP using TiO_2 fixed on a glass plate. Their findings revealed that 92.8% of CIP was removed using an initial CIP concentration of 3 ppm after 105 min. Nguyen et al. [32] studied the CIP removal process under UV–visible light using nitrogen-modified S-TiO_2. The sol–gel method was employed to load the catalyst with N and S. The study revealed that 78.7% of CIP was removed was using a 30 ppm initial concentration of CIP. Manasa et al. [33] found that photodegradation of CIP in an aqueous solution under sunlight was effective after loading TiO_2 with cerium and boron. Although the use of Ce-TiO_2 produced a better removal efficiency than B-TiO_2, when Ce-TiO_2 and B-TiO_2 catalysts were used together, removal efficiencies of 90–93% were obtained.

This work aims to investigate the removal of CIP using PCP with a commercial TiO_2 catalyst in suspended form with the feed. The TiO_2-based catalyst was functionalized by doping it with nitrogen using the co-precipitation method. The performance of the TiO_2 catalyst doped with nitrogen was tested under optimal operating conditions. The performance was tested in two forms: suspension with feed, and coated form. Experimental design and statistical analysis were used in this work for optimizing the operating parameters of PCP using the response surface methodology (RSM) technique, and the statistical analysis was based on an analysis of variance (ANOVA). This technique is considered to be a useful, highly effective, and popular experimental design approach. It has the benefit of enabling the quantification of significant and responsive variables, first-order and second-order terms, and the parameters' interaction terms.

2. Results and Discussion

2.1. The Characteristics of the N-Doped TiO_2 Catalyst

2.1.1. Energy-Dispersive Spectroscopy (EDS)

EDX was employed to examine the composition of the catalytic material. The Ti atoms, O atoms, and impurity contents on the sample surface were measured at different spots on the TiO_2 surface. Figure 1a depicts the EDS spectra of the net TiO_2 peaks, which include 51.9 wt% Ti and 43.0 wt% O. Meanwhile, Figure 1b depicts the presence of nitrogenous metal in traces of TiO_2 at 5.0 wt%, in addition to the main contents of 50.1 wt% Ti atoms and 40.1 wt% O atoms. As a result, this research proves that nitrogen atoms have an effect on the TiO_2 lattice and confirms that nitrogen is present both inside and on the surface of TiO_2 particles [34,35].

Element	Atomic %	Atomic % Error	Weight %	Weight % Error
C	10.1	0.4	5.1	0.2
N	0.1	0.1	0.0	0.0
O	64.0	1.6	43.0	1.1
Ti	25.8	0.1	51.9	0.3

Figure 1. *Cont.*

Element	Atomic %	Atomic % Error	Weight %	Weight % Error
C	9.1	0.3	4.7	0.2
N	8.5	0.8	5.1	0.5
O	58.1	1.4	40.1	0.9
Ti	24.2	0.1	50.1	0.3
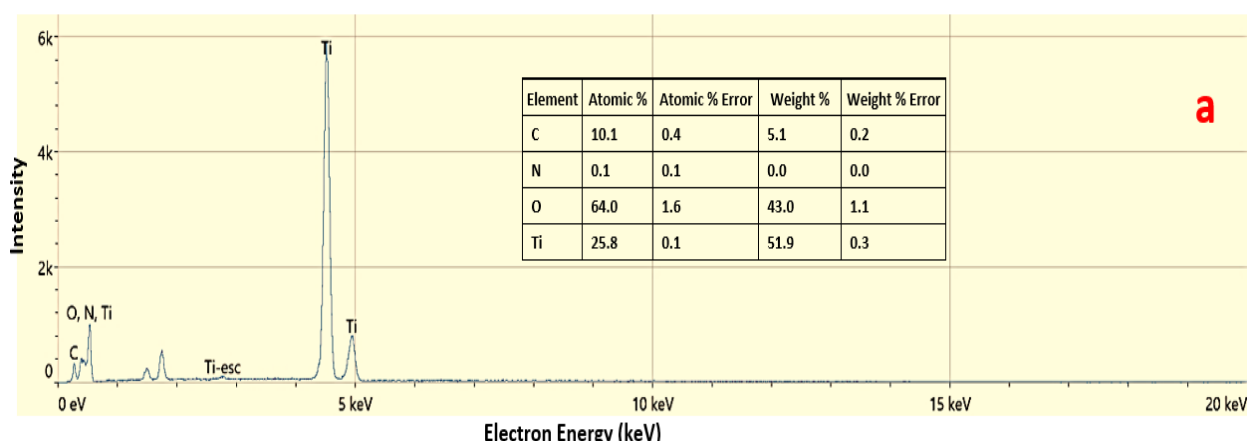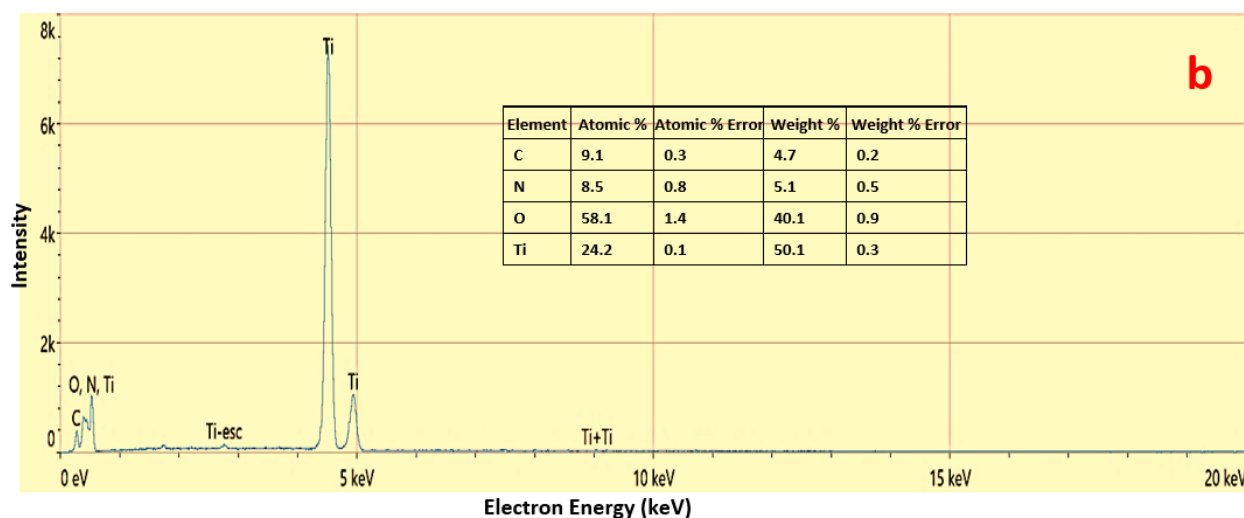
Figure 1. The EDS spectra showing the composition of (**a**) net TiO_2 and (**b**) 5.0 wt% $N\text{-}TiO_2$.

2.1.2. Scanning Electron Microscopy (SEM)

The morphological and structural characteristics of the catalyst have a significant impact on the photocatalytic activity. Figure 2a depicts the net TiO_2 SEM images with a magnification of 2400, 2500, and 5000× (50, 40, and 20 μm, respectively), while Figure 2b depicts the 5 wt% $N\text{-}TiO_2$ SEM images with a magnification of 2400, 2500, and 5000× (50, 40, and 20 μm, respectively). The photocatalytic activity of the nanocomposite was increased due to the additional continuous link between the nanoparticles and nitrogen, allowing the passage of charge carriers during the photocatalysis [20]. It can be seen from Figure 2a that the aggregation of net TiO_2 is mostly made up of many irregular spherical-shaped TiO_2 nanoparticles, which are observed to have agglomerated, probably due to the calcination at 450 °C. However, a visible difference can be seen between the pristine TiO_2 depicted in Figure 2a and the N-doped TiO_2 particles depicted in Figure 2b. The cluster-like shape formed by the N-doped TiO_2 could be due to morphological changes as a result of the nitrogen molecules chemically adhering to the TiO_2 particles. The doping of the TiO_2 with nitrogen could have induced smaller nanoparticles with good dispersibility, which could enhance the photoactivity of the TiO_2 catalyst in the degradation of the CIP from wastewater [31,34].

2.1.3. Fourier-Transform Infrared (FTIR) Spectroscopy

The FTIR transmission spectra represented by a wavelength range of 500–5000 cm^{-1} are depicted in Figure 3a,b. The peaks below 500 cm^{-1} and 1344 cm^{-1} correspond to the titanium crystal lattice vibration in the anatase form, which includes Ti-O bonds, Ti-O-Ti bonds, and O-Ti-O bonds [20,36,37]. The strongest indication of N's existence in TiO_2 is when the first band of net TiO_2 shifts from 459.06 cm^{-1} to 516.92 cm^{-1}. The absorption peaks in 3400–3500 cm^{-1} and 1600 cm^{-1} are caused by the stretching and bending vibrations of the physisorbed water molecules (OH) on the catalyst surface, respectively [32]. These peaks were observed to be wider for $N\text{-}TiO_2$ compared to TiO_2, increasing the capacity to produce oxidizing species such as hydroxyl radicals in the photocatalytic degradation of antibiotic compounds. The N-doped TiO_2 contains two Ti-O-N-bond-related absorbance peaks in the 1054 and 1130 cm^{-1} range, in contrast to pure TiO_2 [32,33]. In undoped TiO_2, these peaks are absent. The FTIR measurements show that N can be found in TiO_2 in both interstitial and substitutional forms.
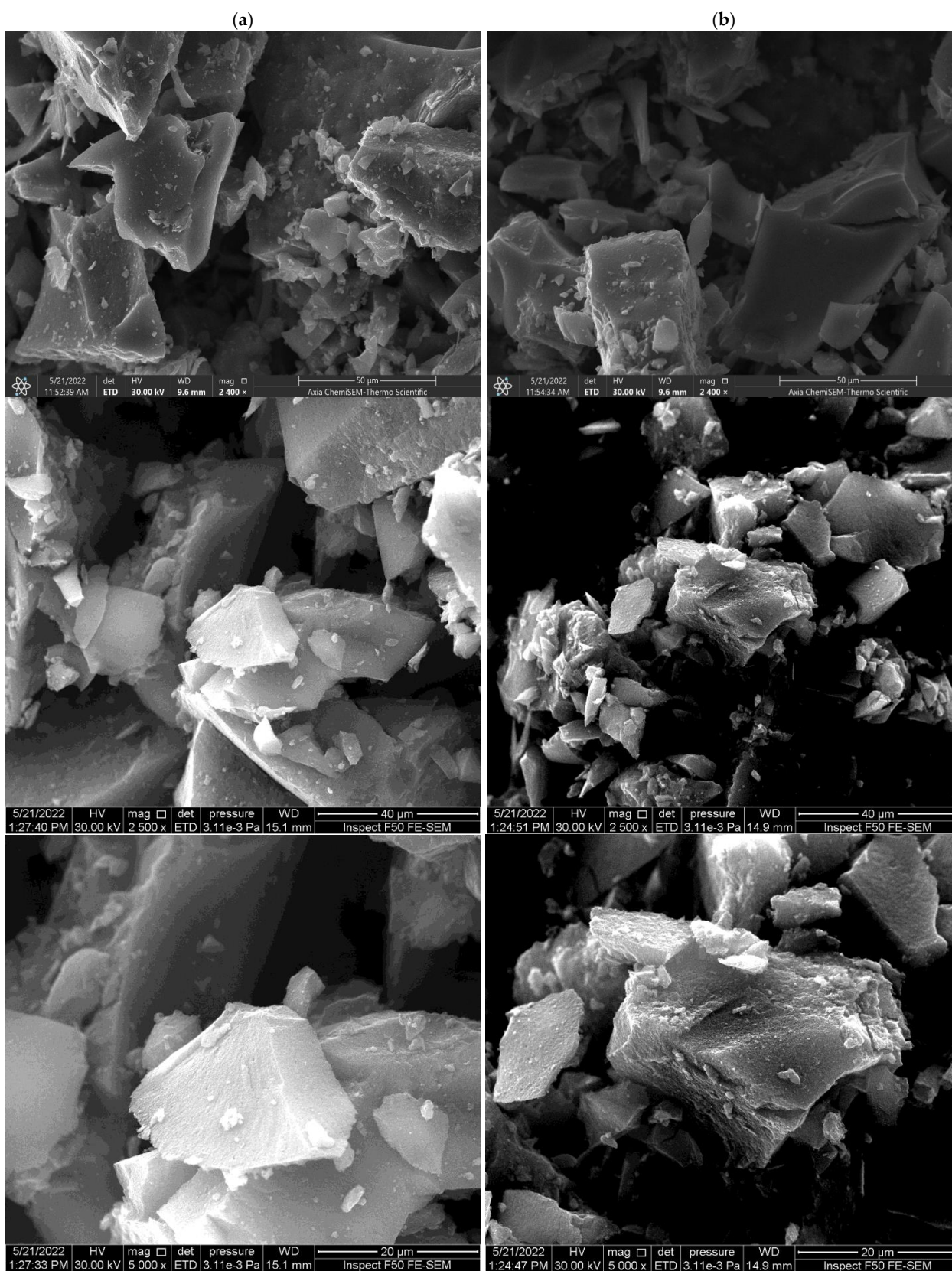
(**a**)   (**b**)

Figure 2. SEM images at various sizes of (**a**) net TiO_2 and (**b**) 5 wt% N-doped TiO_2.
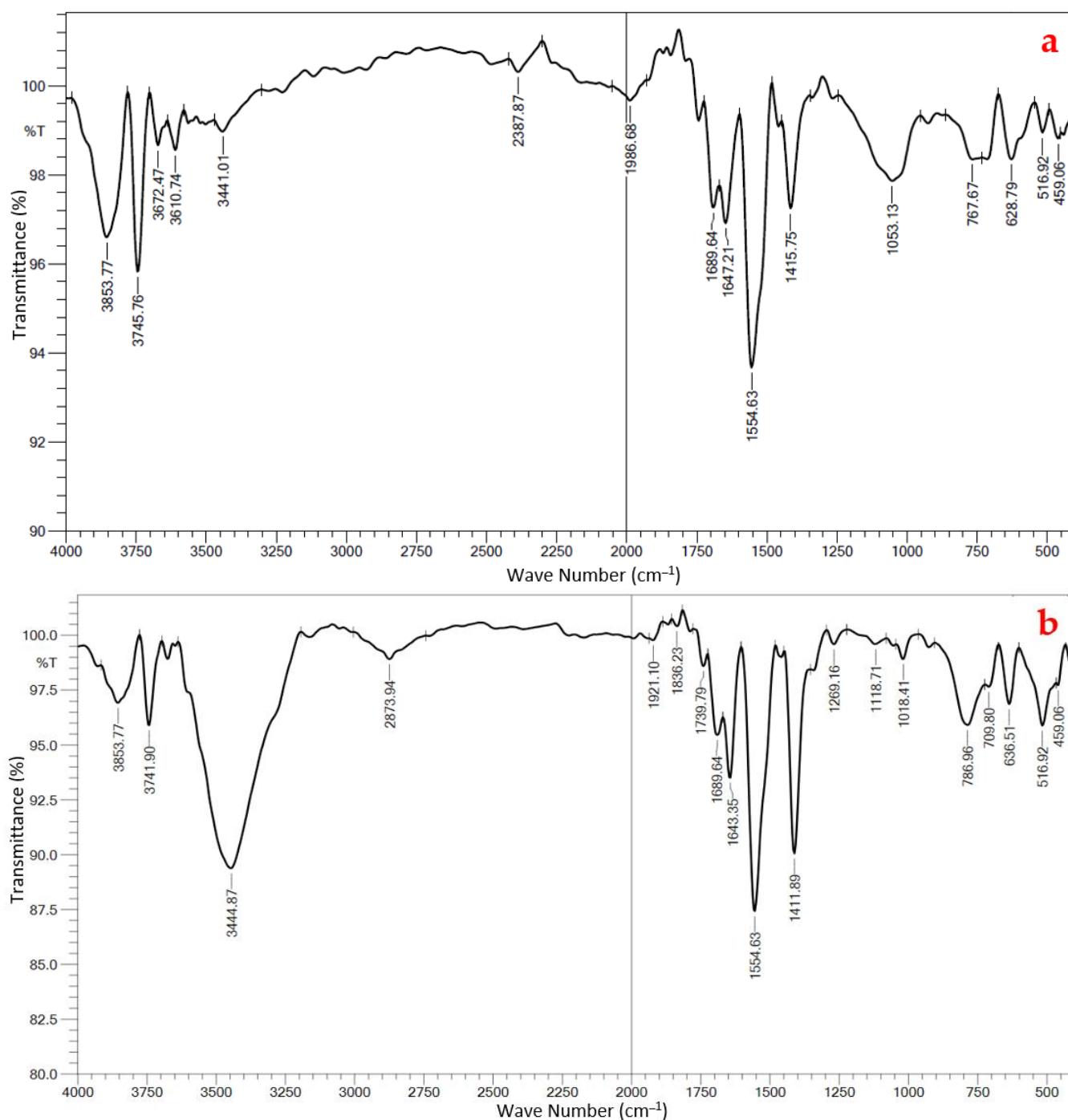
Figure 3. FTIR spectra of nano-TiO$_2$: (**a**) net TiO$_2$; (**b**) 5 wt% N-doped TiO$_2$.

It can be seen that the increase in the N doping on the TiO$_2$ catalyst resulted in the bandgap energy and wavelength shifting from the UV region to the visible region. At a wavelength of 386 nm, the pure TiO$_2$ had a bandgap energy of 3.21 eV, while the 5 wt% N-doped TiO$_2$ had a bandgap energy of 2.27 eV. The link between CIP concentration and contact time may cause this phenomenon. When the concentration is low at a specific time, it is challenging for the photocatalysts to contact the CIP molecules to initiate the process. The FTIR spectroscopic comparison of the N-doped and pristine nano-TiO$_2$ is shown in Figure 3. As can be seen, for the 5 wt% N-TiO$_2$, the peaks correspond to the stretching and bending vibrations of the OH group caused by the water molecules. It can be seen that a wavelength of 3853.77 cm^{-1} was observed for the 5 wt% N-TiO$_2$. A broad absorption

band related to the N-O oscillations was visible for 5 wt%. With a wide absorption range between 1554.6 and 1643.35 cm^{-1}, the broad absorption range was between 1500.62 cm^{-1} and 1554.6 cm^{-1}. However, it was significantly different from the other doping samples. These results show that pure TiO_2 has a larger band number of OH groups on the FTIR diagram than N-TiO_2.

2.2. Photocatalytic Degradation of CIP with Nano-TiO_2

2.2.1. Photocatalytic Degradation with the Suspension of Net TiO_2

Figure 4 shows the timing performance of PCP for the degradation of CIP by using a net TiO_2 catalyst in suspension form with the simulated solution. The CIP removal was 87.8% under the influence of UV rays at the best operating conditions (i.e., initial concentration of CIP = 30 ppm, pH = 5, feed flow rate = 0.4 L/min). The analysis of the CIP removal efficiency was carried out every 15 min to determine the best removal efficiency after two hours. The changes in the bandgap energy can be calculated based on the equation $Eg = 1239.8/\lambda$, where Eg is the sample's bandgap energy (eV) and λ (nm) is the effective spectrum's wavelength [18]. The bandgap energy of net TiO_2 is 3.21 eV, and its wavelength is 386 nm.
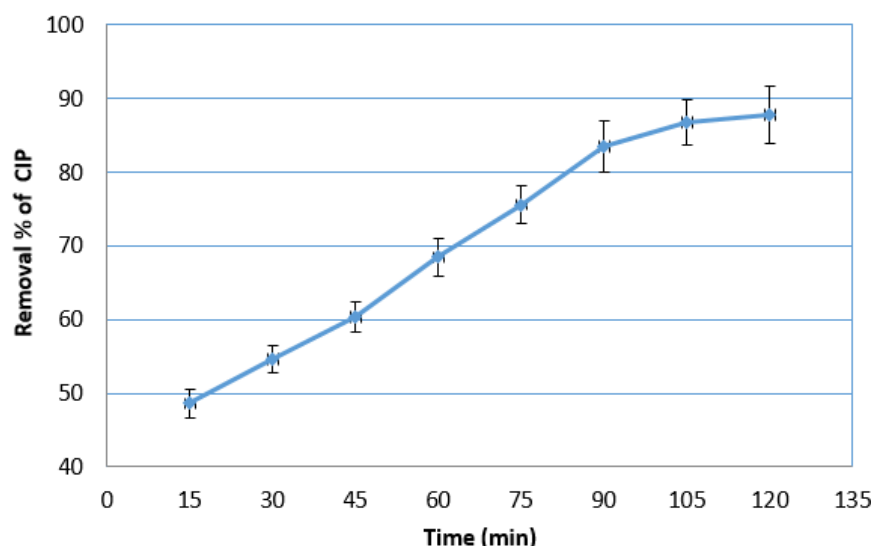

Figure 4. CIP removal percentage using net TiO_2 during testing under optimal operating conditions: initial concentration of CIP = 30 ppm, pH = 5, feed flow rate = 0.4 L/min.

2.2.2. Photocatalytic Degradation with the Suspension of N-Doped TiO_2

The photocatalytic activity of the N-doped TiO_2 as a function of the CIP removal efficiency is depicted in Figure 5. It can be seen that the CIP removal efficiency was influenced by the N doping on the TiO_2 under the best operating conditions. As shown in Figure 5, an increase in %N doping from 0 to 5.7 wt% significantly improved the CIP removal efficiency, with a maximum value of 93.7% obtained at 5 wt%. According to Nguyen et al. [32], this observation could be due to the effect of N doping on the bandgap energy. The bandgap of the photocatalyst has been observed to decrease with increasing N doping. Moreover, the production of reactive radicals increases with the increase in the amount of photocatalyst, because more active sites lead to faster pollutant removal. However, increasing the weight percentage of N doping beyond 5 wt% decreased the CIP removal efficiency, possibly due to catalyst buildup (particle–particle interaction). This might reduce the total active surface area and light intensity, limiting the degradation efficiency [28,32]. Hence, 5 wt% nitrogen in N-TiO_2 was used to remove the CIP because it produced the best removal efficiency. The 5 wt% N-doped TiO_2 had a bandgap energy of 2.27 eV at 546 nm. This decrease in energy falls into the wavelengths range of visible light [27]. This means that doping TiO_2 with 5 wt% N increases the photocatalyst's energy

efficiency by 29.3%. Figure 6 shows the timing performance of the PCP for the degradation of CIP using a 5 wt% N-TiO$_2$ catalyst in suspension form with the simulated solution.
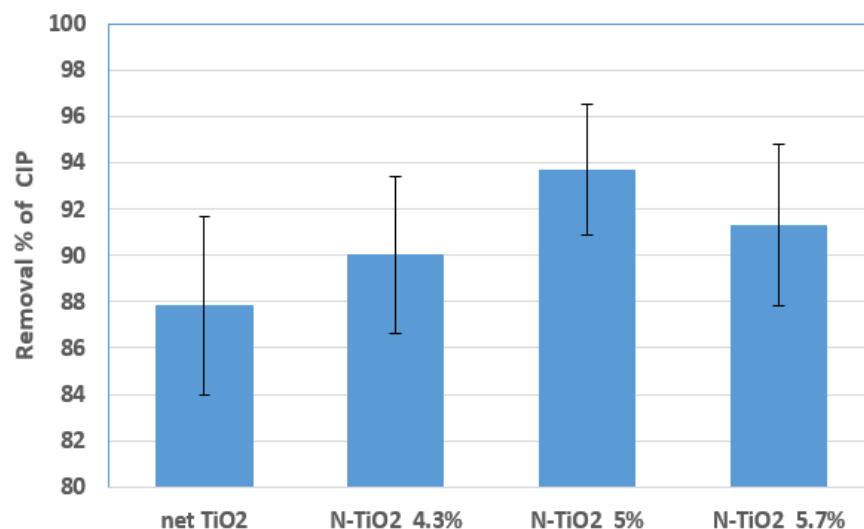

Figure 5. Variation in removal efficiency against wt% N-doped TiO$_2$ at initial concentration of CIP = 30 ppm, pH = 5, and feed flow rate = 0.4 L/min.
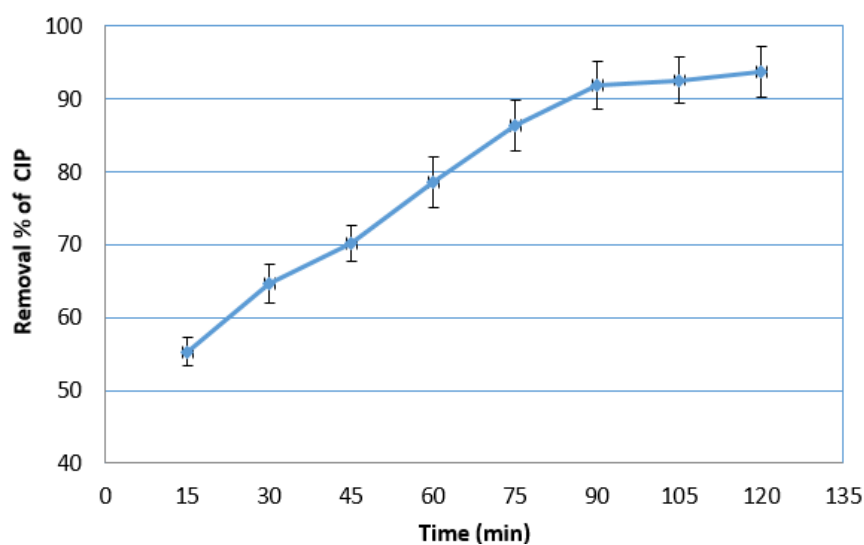

Figure 6. CIP removal percentage using 5 wt% N-TiO$_2$ during testing under optimal operating conditions: initial concentration of CIP = 30 ppm, pH = 5, feed flow rate = 0.4 L/min.

2.2.3. Photocatalytic Degradation with the N-Doped TiO$_2$ after the Coating Process

The 5 wt% N-TiO$_2$ catalyst was employed for the photodegradation of CIP under the best operating conditions after coating the reactor. Figure 7 shows that there was an enhancement in the CIP removal efficiency obtained with the PCP used with the catalyst-coated reactor. The reduction in the bandgap of the catalyst after doping to less than 2.2 eV resulted in an increase in the number of active sites [31].
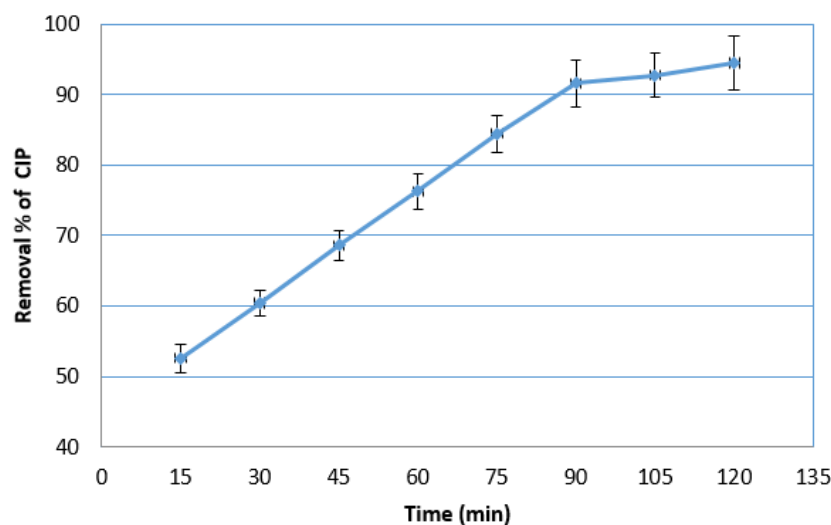
Figure 7. CIP removal percentage using 5 wt% N-doped TiO_2 after the coating process at initial concentration of CIP = 30 ppm, pH = 5, and feed flow rate = 0.4 L/min.

2.3. Effect of the Operating Parameters on the Removal Efficiency

2.3.1. Effect of Initial Ciprofloxacin Concentration

The effects of the initial CIP concentrations of 6–30 ppm on its photocatalytic degradation are shown in Figure 8. It can be seen that there was a significant improvement in the CIP removal efficiency with an increase in the initial concentration from 6 to 30 ppm. It is noteworthy that at a concentration of 30 ppm, the TiO_2 significantly removed the CIP after 120 min. The interaction between CIP molecules and the oxidizing radicals, which are more prominent at lower CIP concentrations, enhanced the photodegradation efficiency in the presence of the catalyst. Due to competition of the CIP particles with the catalyst's active sites and the emergence of intermediate decomposition products, this process was not a linear increase [32]. Hence, it can be seen that the increase in the concentration of CIP increased the removal efficiency to a certain extent. The increase in the concentration of CIP and the number of moles in the reaction environment increased the number of TiO_2 surface sites and caused them to become saturated. This phenomenon prevented effective excitation of the catalyst surface by optical photons and reduced the removal efficiency [35–40]. The high concentration of the diluent caused an increase in the adsorption of the CIP on the surface. This could also be attributed to the effects of higher CIP concentrations in reducing the light transmittance and interference of the solution and decreasing the performance of the photocatalytic process [35,36].
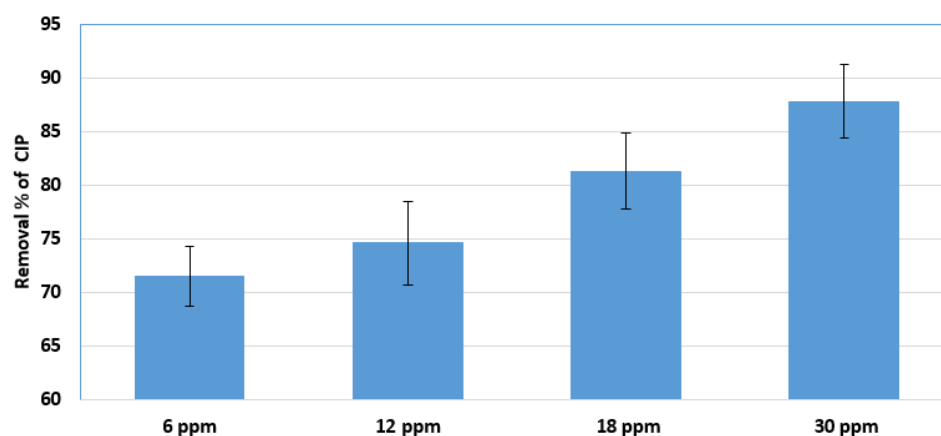

Figure 8. Variation in removal efficiency with the initial CIP concentration at pH = 5 and feed flow rate = 0.4 L/min.

Figure 8 also shows that the maximum CIP removal efficiency of 87.8% was obtained at a concentration of 30 ppm after 120 min. However, when using a concentration of 6 ppm, the removal efficiency became 71.5%. It was also noted that the CIP removal efficiency at 12 ppm was 74.6% at 120 min, while at 18 ppm the CIP removal efficiency was 81.3% at 120 min, which is consistent with the results reported by Soares et al. [41]. However, CIP removal may be more effective at lower doses (30 ppm) in natural aquatic systems, where dilution is more common up to a certain concentration.

2.3.2. Effect of Feed Flow Rate

Another important factor that influences the CIP removal efficiency in the photo-catalytic reactor is the feed flow rate. Different flow rates (0.4–1.5 L/min) were used to investigate the effect of flow rate on the CIP removal efficiency. Figure 9 shows the effects of varying feed flow rates on the rate of CIP degradation. The best removal efficiency of 87.8% was obtained at a lower flow rate of 0.4 L/min for 120 min. Since the CIP has greater chances of adsorption and oxidation at active sites when the residence time is greater, it may be inferred that the CIP removal efficiency from a given volume of test solution increases proportionally with the residence time on the photocatalytic surface. However, researchers use a large variance in the tested flow rates (0.2–2 L/min) [35–44].
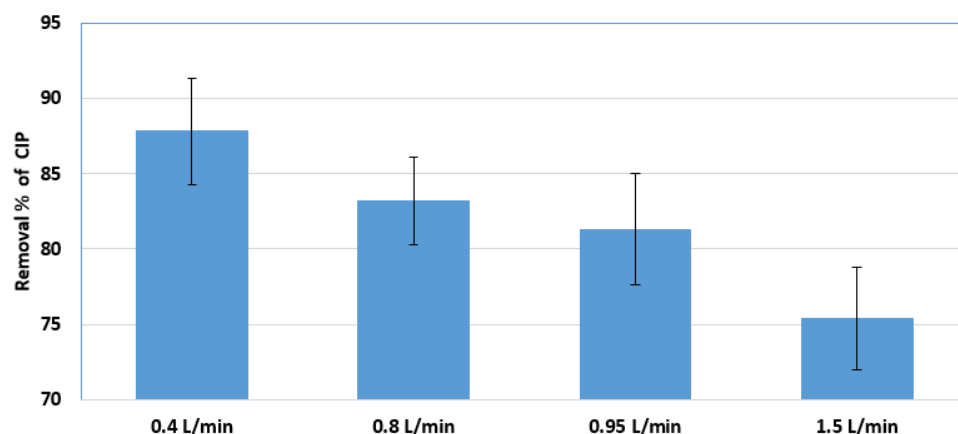

Figure 9. Variation in removal efficiency with flow rate at initial concentration of CIP = 30 ppm and pH = 5.

Figure 9 also shows that the greatest CIP removal at a flow rate of 0.4 L/min was 87.8% at 120 min. The CIP removal was equal to 83.2% at a flow rate of 0.8 L/min, while the CIP removal decreased to 81.3% at a flow rate of 0.95 L/min. The CIP removal further decreased to 75.4% at a flow rate of 1.5 L/min, which was the lowest removal efficiency. At a higher feed flow rate, the penetration time and removal efficiency can be reduced, because the flow rate is greatly influenced by the penetration time, saturation time, and the shape of the penetration curve [35]. The higher flow rate reduces the effective contact time between the adsorbent surface and the absorbent particles, as well as the diffusion of the particles, removing less CIP, which is consistent with the findings of Nakarmi et al. [45].

2.3.3. Effect of pH

The pH of the medium also determines the ionic species of CIP—a molecule with several ionic functional groups—and the electrical charge of the catalyst surface. The photocatalytic degradation of the CIP was examined at a pH of 3–9, as shown in Figure 10. The degradation efficiency of CIP tends to increase gradually in acidic environments (pH 3–5), peaking at pH 5 (normal solution pH), and then slowing down in neutral and alkaline environments (i.e., pH of 6–9). This can be attributed to the low-pH conditions having a higher potential for the oxidation of hydroxyl radicals compared to an alkaline medium [32]. This observation is consistent with the literature [46,47] describing the

removal of CIP using visible-light photocatalysis. At pH of 3, 5, 7, and 9, CIP removal efficiency of 68.8%, 87.8%, 70%, and 10% was obtained, respectively. As a result, the repulsion effect caused a decrease in the removal efficiency at pH 3 and a decrease from pH 7 to 9. Due to the dipole force generated by the positively charged carboxylic groups on the surface of TiO_2, the maximum removal efficiency can be explained by the catalytic degradation of CIP at pH 5 [41]. Moreover, the generation of a hydrogen peroxide (H_2O_2) as a strong oxidizing agent required to minimize the CIP could also enhance the removal efficiency, as reported by Xue et al. [48]. It is noteworthy that the photocatalytic degradation of the CIP from the simulated wastewater is more effective when the pH is higher than 4.88. Given that the pKa value of CIP is 8.7, when the pH of the solution is 5–6, the results obtained are consistent with our findings [49].
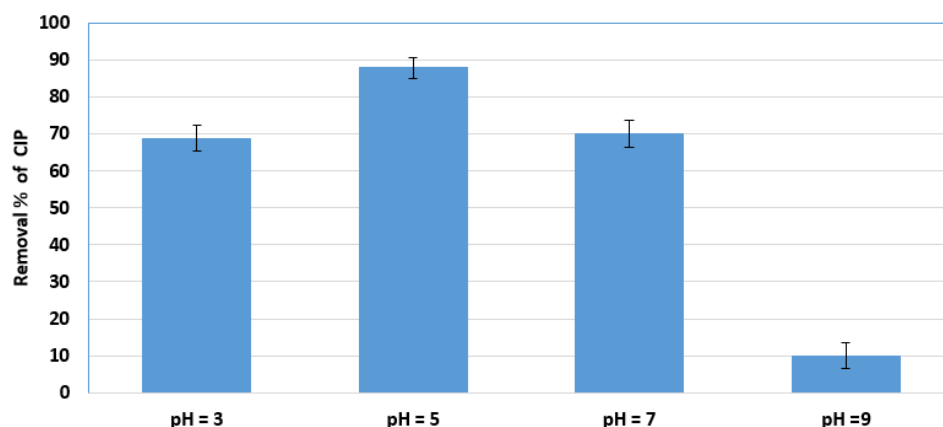

Figure 10. Variation in the removal efficiency of CIP with pH at initial concentration of CIP = 30 ppm and feed flow rate = 0.4 L/min.

Table 1 shows the comparison between the present work and previous studies on the performance of PCP used for the photocatalytic degradation of CIP in simulated aqueous solutions under different operating conditions. CIP removal efficiency of 94.5% was obtained in this study after 120 min of photodegradation activity using 5 wt% N-TiO in a coated form, which is comparable with the results reported in the literature. Gad-Allah et al. [28] reported 95% removal efficiency for CIP after 120 min of photodegradation activity under sunlight at a pH of 5.8. This high CIP removal efficiency could be attributed to the increase in the initial concentration of CIP, which is consistent with the trend obtained in this study. Hence, it can be inferred that there was a direct relationship between the initial concentration of the CIP and the removal efficiency. Conversely, Durán-Álvarez et al. [29] reported a removal efficiency of 63% even though a metal-laden photocatalyst was used at an initial CIP concentration of 30 ppm. This low CIP removal could be attributed to the possible effect of using a medium with pH 6.1. As previously stated, the closer the pH is to neutral, the lower the removal rate, since the CIP needs an acidic environment to produce pollution. Malakootian et al. [31] employed a coating process for a net catalyst on a glass plate to obtain a CIP removal efficiency of 92.8%. The differences in the CIP removal efficiency obtained in this study and that reported by Malakootian et al. [31] could be due to the variation in the initial concentration of the CIP. Zheng et al. [30] modified a TiO_2-based catalyst with graphite, and the initial concentration was higher than what was used in this study. Nevertheless, the CIP removal efficiency reported by Zheng et al. [30] did not exceed 94%. Nguyen et al. [32] reported a CIP removal efficiency of 78.7% even though they used a photocatalyst modified with sulfur and nitrogen. The differences between the CIP removal efficiency reported in this study and that reported by Nguyen et al. [32] could be due to the variation in the weight percentage of the elements doped on the TiO_2 catalyst, since increasing the doping percentage beyond a certain level could lead to more production of hydroxyl radicals. This might cause an increase in the pollutant intermediates, reducing the light intensity on the catalyst and, thus, reducing the removal

rate. Furthermore, Manasa et al. [33] observed that the use of B-TiO$_2$ and Ce-TiO$_2$ catalysts increased the CIP removal efficiency up to the range of 90–93% under sunlight and at an initial CIP concentration of 40 ppm and pH of 5.5–6. Hence, the increased removal rate could be attributed to the reduction in the bandgap of pristine photocatalyst to a point allowing for the rapid and superior degradation of the CIP.

Table 1. Comparison of the operating conditions and the percentages of CIP removal for the current work and various previous studies.

Conc. of CIP (ppm)	Conc. of Catalyst (mg/L)	Catalyst Type-Form	pH	λ_{max} (nm)	Time (min)	R (%)	Ref.
50	1000	Net-TiO$_2$-Sus.	5.8	Sunlight	120	95	[28]
30	500	Au-TiO$_2$-Sus.	6.1	254	180	63	[29]
15	350	GMC-TiO$_2$-Sus.	5.8	254	90	94	[30]
3	1000	Net-TiO$_2$-Cot.	5	276	105	92.8	[31]
30	2000	S,N-TiO$_2$-Sus.	5.5	276	180	78.7	[32]
40	500	B-TiO$_2$-Sus. Ce-TiO$_2$-Sus.	5.5–6	276	180	90–93	[33]
30	1000	N-TiO$_2$-Cot.	5	257	120	94.5	present work

Conc. = concentration, GMC = graphitized mesoporous carbon, S = sulfur, N = nitrogen, B = boron, Ce = cerium, Sus. = suspension, Cot. = coated, λ_{max} = wavelength.

The conduction band (CB) energy of TiO$_2$ anatase (with a bandgap E_g = 3.2 eV) is −0.51 V at neutral pH, while the valence band (VB) energy is 2.69 V under the same conditions. This means that the CB energy level is more negative than the potential of oxygen reduction ($E(O_2/{\cdot}O_2^-)$ = −Ve), and that the VB energy level is more positive than the potential of water oxidation ($E(H_2O/OH^-)$ = +Ve). This makes it possible to obtain highly reactive oxidizing species such as superoxide radicals (${\cdot}O_2^-$) and hydroxyl radicals (${\cdot}OH$) in the photocatalytic process over TiO$_2$. The degradation mechanism of CIP using TiO$_2$ proceeds via the formation of e^-/h pairs upon illumination with energy greater than or equal to 3.2 eV [31]. Therefore, the photocatalytic process itself is initiated when TiO$_2$ absorbs a photon from the light source with energy (h_v) equal to or greater than the bandgap (E_g) of the photocatalyst. In general, a photocatalytic process over TiO$_2$ comprises the following stages:

1. Adsorption of CIP on the TiO$_2$ surface;
2. The photocatalytic degradation of the adsorbed CIP via oxidation–reduction reactions with photogenerated electrons (e^-), holes (h^+), and reactive species (depicted in Figure 11);
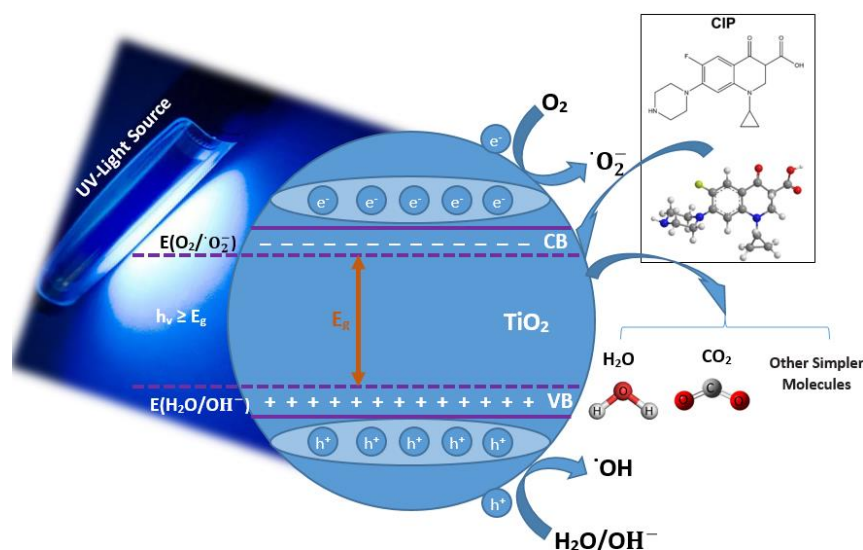3. Desorption of degradation products.

Figure 11. The proposed mechanism for the degradation of CIP using N-TiO$_2$.

2.4. Design-Expert Software Results

Table 2 presents the details of the various combinations of the independent variables, namely, the initial CIP concentration, the pH of the medium, and the flow rate. Altogether, there were 20 runs employed with each combination of the independent variables to obtain a corresponding response variable, i.e., the removal efficiency of the CIP (R%).

Table 2. Experimental data points and responses used in the CCD.

Std	Run	Con. (ppm)	pH	Flowrate (L/min)	R (%)
17	1	18	5	0.95	81.3
20	2	18	5	0.95	81.3
6	3	30	3	1.5	62.5
13	4	18	5	0.4	80.4
15	5	18	5	0.95	81.3
3	6	6	7	0.4	44.5
5	7	6	3	1.5	51.7
1	8	6	3	0.4	55.0
10	9	30	5	0.4	87.8
9	10	6	5	0.95	71.5
2	11	30	3	0.4	68.8
18	12	18	5	0.95	81.3
19	13	18	5	0.95	81.3
15	14	18	5	0.95	81.3
14	15	18	5	1.5	75.4
8	16	30	7	1.5	66.8
11	17	18	3	0.95	60.0
7	18	6	7	1.5	42.6
12	19	18	7	0.95	65.8
4	20	30	7	0.4	70.0

The combination of the independent variables and corresponding responses obtained from the experimental runs were analyzed via ANOVA to determine the statistical significance of each factor. Table 3 shows the details of the ANOVA results, with the F-value and *p*-value for each independent variable. The ANOVA helps to determine whether the responses obtained from the experimental runs are statistically significant or not [50]. The F-value of 101.29 implies that the predicted model is significant. Based on the *p*-values, the initial CIP concentration ($p < 0.0001$) has a more significant effect on the CIP removal efficiency compared to the pH of the medium ($p = 0.1995$) and the flow rate ($p = 0.0079$). It can be seen that the pH of the medium does not have any statistical influence on the CIP removal efficiency. A *p*-value less than 0.05 indicates that the model is significant. In this case, A, C, AB, B^2, and C^2 are significant model terms [51]. Meanwhile, *p*-values greater than 0.1 indicate that the model terms are not significant. If there are many insignificant model terms (not counting those required), model reduction may improve this model.

Table 3. Results of ANOVA for the experiments of Table 2.

Source	SS	df	Mean Square	F-Value	*p*-Value
Model	3328.09	9	369.79	101.29	<0.0001
A ≡ concentration	796.65	1	796.65	218.22	<0.0001
B ≡ pH	6.89	1	6.89	1.89	0.1995
C ≡ flow rate	39.90	1	39.90	10.93	0.0079
AB	78.75	1	78.75	21.57	0.0009
AC	2.19	1	2.19	0.5989	0.4569
BC	2.53	1	2.53	0.6934	0.4245
A^2	3.12	1	3.12	0.8536	0.3773
B^2	1047.05	1	1047.05	286.80	<0.0001
C^2	33.47	1	33.47	9.17	0.0127

2.4.1. Graphical Interpretation by 2D and 3D Response Surfaces

The best combinations of the independent variables that would help the photocatalytic reaction can be determined with the help of response surface optimization. In this study, three variables were examined to determine the best conditions under which CIP removal could be optimized to determine the ideal operating conditions to ensure minimal levels of contamination during the photocatalysis process. Contour plots and three-dimensional (3D) response surface plots were employed to analyze the influence of the independent variables on the response, since the dependent variable was plotted for two explanatory factors while holding the remaining variables constant in 3D response plots. Figure 12a,b show the graphical representation of the contour and 3D plots for the interaction effects of the various independent variables on the response. The response surface plots depict a couple of subfigures that reveal the response behavior under two operating conditions, with the other factors held constant.
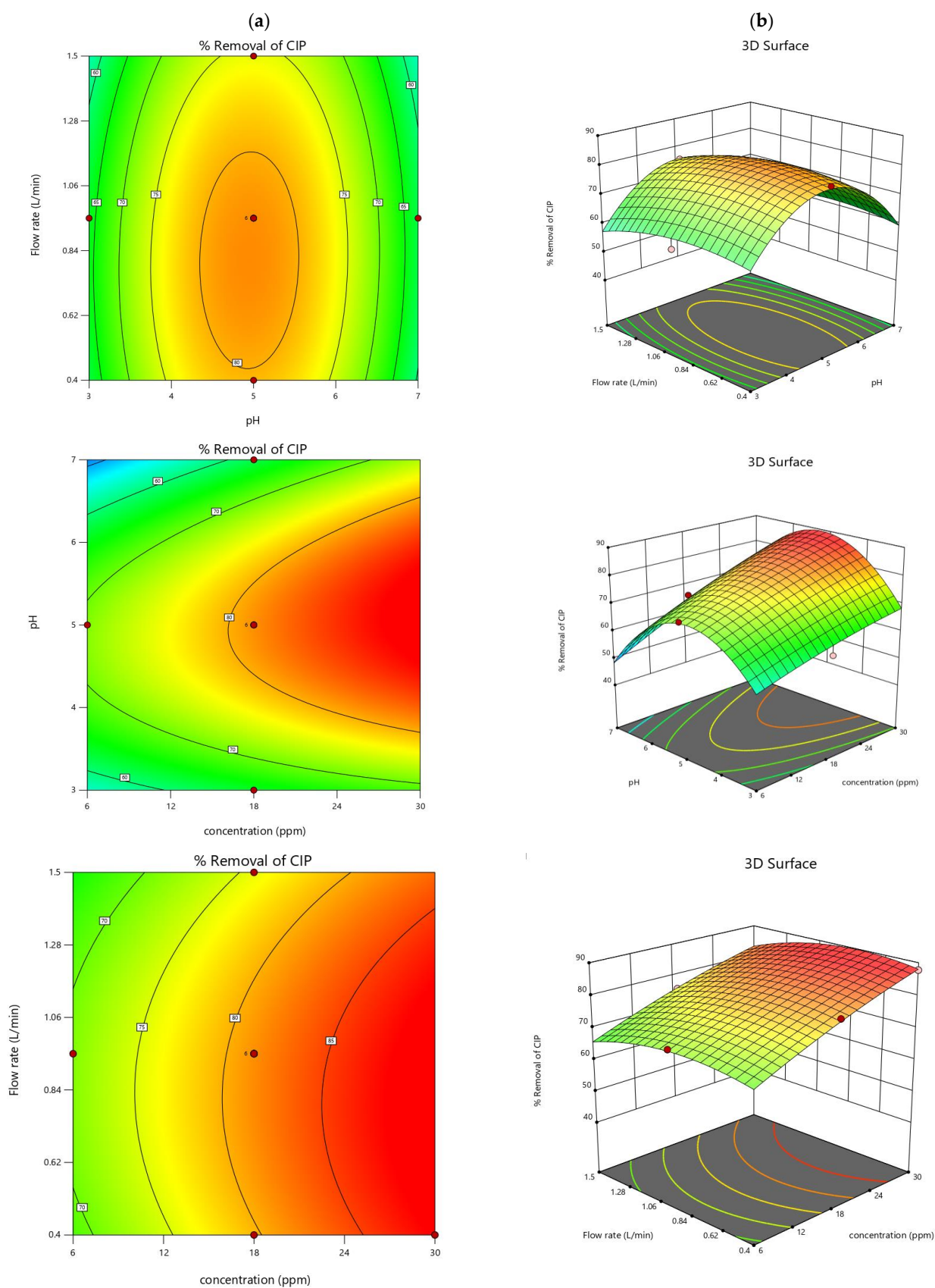
(a)

(b)

Figure 12. Interactive effects of pH, initial concentration, and flow rate on the removal efficiency of CIP: (**a**) Two-dimensional (2D) response surface perimeters. (**b**) Three-dimensional (3D) response surface perimeters.

The results show that the removal efficiency of CIP tended to increase gradually in acidic environments (pH of 3–5), peaking at pH 5 (the solution's natural pH), and then decreasing in neutral and alkaline environments (pH of 6–9). The maximum CIP removal efficiency was obtained at a flow rate of 0.4 L/min, photodegradation time of 120 min, initial CIP concentration of 30 ppm, and pH of 5.

2.4.2. Predicted Model

Based on the optimal conditions of the independent variables, the RSM model depicted in Equation (1) was employed to predict the CIP removal efficiency. This equation showed the appropriate mathematical formula (i.e., regression) for finding the response values (R%) through the coefficients of the affected factors found.

$$R\% = 81.42 + 9.19\,A - 0.83\,B - 1.94\,C + 3.14\,AB - 0.5053\,AC + 0.5625\,BC - 1.23\,A^2 - 18.65\,B^2 - 3.78\,C^2 \tag{1}$$

Figure 13 shows the predicted versus actual plot for the CIP removal efficiency. Thus, in terms of coded factors, Equation (1) can be used to predict the response for a given level of each factor. By default, the high levels of factors are coded as +1, while the low levels are coded as –1. The coded equation is useful for determining the relative impacts of the factors by comparing the factor coefficients [51].
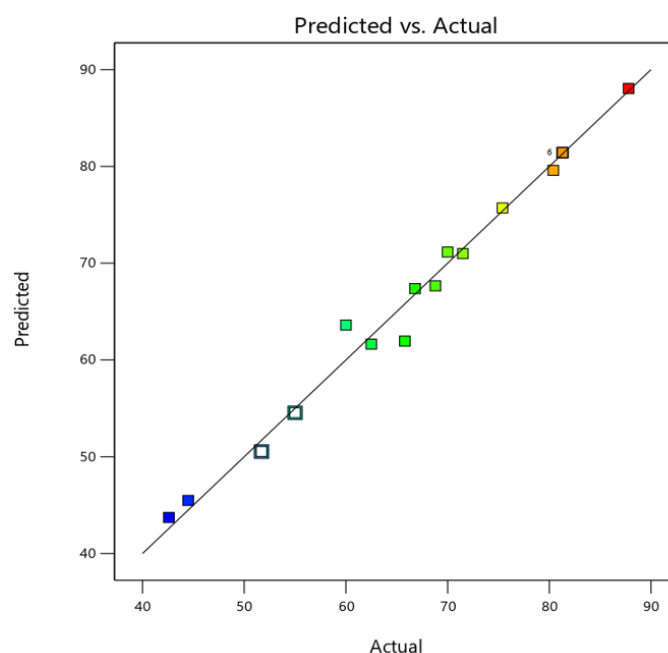

Figure 13. Diagnostic of predicted values vs. actual values for CIP removal %.

3. Materials and Methods

3.1. Materials

The chemicals used in this study include ciprofloxacin hydrochloride ($C_{17}H_{18}FN_3O_3 \cdot HCl$) (CIP) (Mwt. 367.84 and wavelength λ_{max} = 272 nm) supplied by Micro Labs Limited, India; nano-TiO_2 (anatase) of 79.87 Mwt., 99% purity, 3.2 eV bandgap energy, and 30–50 nm particle size, supplied by Hongwa International Group Ltd., Guangdong, China; titanium (IV) isopropoxide (TTIP) with 97% purity, from Sigma-Aldrich, India; ammonium hydroxide (NH_4OH) with about 25% NH_3, supplied by Thomas Baker, India; nitric acid (HNO_3) from Alpha Chemika, India; and hydrochloric acid (HCl) of 35–38% concentration and sodium hydroxide (NaOH), from Thomas Baker, Mumbai, India.

3.2. Methods

3.2.1. Preparation of N-Doped TiO$_2$

This stage involved the preparation of various weight ratios of nitrogen-doped TiO$_2$ by the co-precipitation method. In this method, 2 mL of titanium(IV) isopropoxide (TTIP) was added to 50 mL of distilled water and constantly stirred for 10 min using a magnetic stirrer to obtain a white suspension. While still being continuously mixed, 20 mL of nitric acid (65%) was added to the white suspension, converting it to a transparent slurry. Then, 85 mL of ammonium hydroxide (25% purity) was slowly added to the solution and mixed for 60 min with a magnetic stirrer to obtain a white precipitate again. Vacuum filtration was used to obtain a white precipitate from the final mixture, which was then left to dry at room temperature for 24 h. Then, the dried N-TiO$_2$ was calcined in an oven at 450 °C for two hours. Finally, after cooling down, the extracted powder was crushed to a desirable particle size before being used [34].

Different quantities and concentrations of titanium isopropoxide, nitric acid, and ammonium hydroxide were used in the catalyst doping to obtain various ratios (4.3 wt% to 5.7 wt%) of nitrogen-to-catalyst doping (N-TiO$_2$).

3.2.2. Coating Process Using the Nitrogen-Doped Catalyst

The coating process was carried out with a varnish applied to the surface of a galvanized iron sheet with dimensions of 28 cm × 14 cm, and then the N-TiO$_2$ nanocatalyst was manually sprayed. This was carried out using a 5 wt% N-TiO$_2$ catalyst because it achieved higher pollutant removal than other doping ratios when used in suspension form. The mixture was ultrasonicated to achieve better stability by avoiding the accumulation of nanoparticles. Finally, we obtained an aqueous solution suitable for spraying on the pallet [31].

The doped catalyst-coated pallet was placed in the photocatalytic reactor and operated for 2 h, with samples drawn every 15 min to determine the percentage removal of CIP. The previous optimal conditions were selected for the new experimental tests.

3.2.3. Analysis Methods

Smart SCAN technology was used with an INSPECT f50 scanning electron microscope (SEM, Holland) at an accelerating voltage of 200 V–30 kV to identify the surface morphological parameters. Energy-dispersive spectroscopy (EDS, USA) was employed to determine the elemental composition of the catalyst. Fourier-transform infrared spectroscopy (FTIR, Japan) (Model: 1800, high performance) was used to determine the photocatalyst's functional groups.

3.2.4. Experimental Setup

The photodegradation experiments were performed using synthetic industrial wastewater prepared by mixing 500 mL of tap water with the desired concentration of CIP. The CIP concentrations considered in the present work were 6–30 ppm. The TiO$_2$ (1000 ppm) was added to the synthetic wastewater and stirred continuously using a magnetic stirrer for 1 h, with the acidity of the mixture adapted by adding a small amount of HCl. Then, a circulating pump was used to transfer the contaminated water (i.e., the simulated solution) to a tilted glass slide exposed to UV rays (photocatalytic reactor). UV irradiation at 275 nm and light intensity of around 2 W/m^2 were used. The samples were collected through a bypass valve (each sample = 10 mL) every 15 min after exposure to UV light to obtain a batch style of CIP removal for 2h. Then, the removal efficiency of the CIP was analyzed for each experiment. The reported values of this work were averaged over three measurements. The degradation efficiency was also calculated from Equation (2) [20]:

$$R\% = (C_0 - C)/C_0 \times 100 \qquad (2)$$

where C_0 is the initial concentration of CIP (ppm), and C is the CIP concentration (ppm) at reaction time t.

The experiments were carried out to study the effects of the operating parameters (i.e., flow rate, pH, and initial concentration of CIP) on the decomposition efficiency (i.e., CIP removal percentage). The experimental rig photo and diagram are depicted in Figure 14.
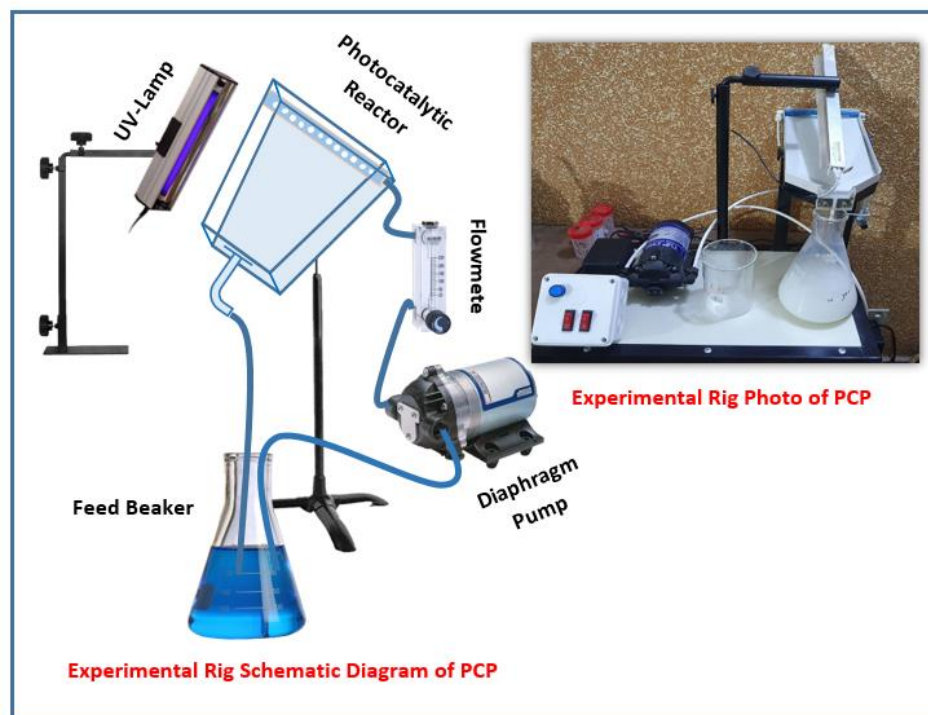

Figure 14. The experimental device used in the photocatalytic process (photo and diagram).

3.2.5. Experimental Design and Optimization Studies

Design-Expert Version 12 was used in the present investigation for the experimental design and response surface optimization study. The most popular fractional factorial design employed in the response surface model is the central composite design (CCD). A set of axial points known as the star points are added to the center points in this design. First-order and second-order terms can be approximated quickly with this design. In this design, the center points are augmented with a group of axial points called star points, which aid in identifying the nonlinear behavior of the effect and choosing the optimal arrangement of experimental variables to yield the best results with the fewest trial runs required. Design-Expert offers integrated designs, mixed designs, flexible parameter design, inspection, characterization, and optimization, making it useful for determining the number of trial runs required, and it uses analysis of variance (ANOVA) to assess the statistical significance of different components. The user is assisted in selecting the optimal values for the variables of each experiment by a numerical optimizer based on the tested predictive models.

Design-Expert also outputs several graphics to evaluate the residuals. The program calculates the direct effects of each factor and their interrelationships by changing the values of all components in a lump sum. Through the use of this program, the highest and lowest values can be entered for each variable in the photocatalytic process. As a result, it can be used to obtain optimal conditions with few experiments and effectively shorten the trial period. To determine the best conditions for the process with the fewest experiments, at the lowest cost, and in the shortest amount of time, the program finds the ideal experiments by linking the variables used to determine the best conditions based on

the initial concentration of CIP (6–30 ppm), the pH (3–7), and the flow rate (0.4–1.5 L/min). Thus, the main elements as they appeared in the design table are listed in Table 4.

Table 4. Experimental range of parameters in the oxidation process.

Operating Conditions	Low	High
Initial concentration (ppm)	6	30
pH	3	7
Flow rate (L/min)	0.4	1.5

4. Conclusions

This study investigated the application of N-doped TiO_2 in the photocatalytic degradation of CIP in simulated wastewater. The various parameters—such as the initial concentration of the CIP, the pH of the medium, and the flow rate—significantly influenced the CIP removal efficiency from the water. The best operating conditions to maximize the CIP removal efficiency were obtained at an initial CIP concentration of 30 ppm, a feed flow rate of 0.4 L/min, a pH of 5, and a photodegradation time of 2 h. Amongst the various catalyst doping levels investigated, the 5 wt% N-TiO_2 displayed the best performance in suspension form, leading to 93.6% CIP removal efficiency. Overall, 94.5% CIP removal efficiency was obtained for the coated 5 wt% N-TiO_2 on an iron plate. Thus, the best CIP removal efficiency was obtained using the coated N-TiO_2 catalyst. This was due to the increase in the contact surface area between the UV rays and the CIP pollutant in the presence of the N-TiO_2, increasing the formation of oxidative radicals and, thus, obtaining the best CIP removal efficiency within a short time. This study demonstrates that the effectiveness of TiO_2-based photocatalysts can be improved by doping with nitrogen.

References

1. Brillas, E.; Sirés, I.; Oturan, M.A. Electro-Fenton Process and Related Electrochemical Technologies Based on Fenton's Reaction Chemistry. *Chem. Rev.* **2009**, *109*, 6570–6631. [CrossRef] [PubMed]
2. Lopez, R.; Menendez, M.I.; Diaz, N.; Suarez, D.; Campomanes, P.; Ardura, D.; Sordo, T.L. Theoretical studies on the ring opening of β-lactams: Processes in solution and in enzymatic media. *Curr. Org. Chem.* **2006**, *10*, 805–821. [CrossRef]
3. Nikolaous, A.; Meric, S.; Fatta, D. Occurrence patterns of pharmaceuticals in water and wastewater environments. *Anal. Bioanal. Chem.* **2007**, *387*, 1225–1234. [CrossRef]
4. Jayasiri, H.B.; Purushothaman, C.S.; Vennila, A. Pharmaceutically active compounds (PhACs): A threat for aquatic environment. *J. Mar. Sci. Res. Dev.* **2013**, *4*, e122. [CrossRef]
5. Alonso, J.J.S.; El Kori, N.; Melián-Martel, N.; Del Río-Gamero, B. Removal of ciprofoxacin from seawater by reverse osmosis. *J. Environ. Manage.* **2018**, *217*, 337–345. [CrossRef] [PubMed]
6. Sharma, V.K.; Johnson, N.; Cizmas, L.; McDonald, T.J.; Kim, H. A review of the influence of treatment strategies on antibiotic resistant bacteria and antibiotic resistance genes. *Chemosphere* **2016**, *150*, 702–714. [CrossRef]
7. Peng, X.; Hu, F.; Zhang, T.; Qiu, F.; Dai, H. Amine-functionalized magnetic bamboo-based activated carbon adsorptive removal of ciprofoxacin and norfoxacin: A batch and fxed-bed column study. *Bioresour. Technol.* **2018**, *249*, 924–934. [CrossRef]
8. Mekhamer, W.; Al-Tamimi, S. Removal of ciprofloxacin from simulated wastewater by pomegranate peels. *Environ. Sci. Pollut. Res.* **2018**, *26*, 2297–2304. [CrossRef]

9. Grenni, P.; Ancona, V.; Caracciolo, A.B. Ecological effects of antibiotics on natural ecosystems: A review. *Microchem. J.* **2018**, *136*, 25–39. [CrossRef]

10. Huang, Q.; Zhao, J.; Liu, M.; Li, Y.; Ruan, J.; Li, Q.; Tian, J.; Zhu, X.; Zhang, X.; Wei, Y. Synthesis of polyacrylamide immobilized molybdenum disulfide (MoS$_2$@PDA@PAM) composites via mussel-inspired chemistry and surface-initiated atom transfer radical polymerization for removal of copper (II) ions. *J. Taiwan Inst. Chem. Eng.* **2018**, *86*, 174–184. [CrossRef]

11. Huang, Q.; Zhao, J.; Liu, M.; Chen, J.; Zhu, X.; Wu, T.; Tian, J.; Wen, Y.; Zhang, X.; Wei, Y. Preparation of polyethylene polyamine@tannic acid encapsulated MgAl-layered double hydroxide for the efficient removal of copper (II) ions from aqueous solution. *J. Taiwan Inst. Chem. Eng.* **2018**, *82*, 92–101. [CrossRef]

12. Huang, Q.; Liu, M.; Zhao, J.; Chen, J.; Zeng, G.; Huang, H.; Tian, J.; Wen, Y.; Zhang, X.; Wei, Y. Facile preparation of polyethylenimine-tannins coated SiO$_2$ hybrid materials for Cu^{2+} removal. *Appl. Surf. Sci.* **2018**, *427*, 535–544. [CrossRef]

13. Shah, L.A.; Malik, T.; Siddiq, M.; Haleem, A.; Sayed, M.; Naeem, A. TiO$_2$ nanotubes doped poly(vinylidene fluoride) polymer membranes (PVDF/TNT) for efficient photocatalytic degradation of brilliant green dye. *J. Environ. Chem. Eng.* **2019**, *7*, 103291. [CrossRef]

14. Van Tran, T.; Nguyen, D.T.C.; Le, H.T.; Tu, T.T.; Le, N.D.; Lim, K.T.; Bach, L.G.; Nguyen, T.D. MIL-53 (Fe)-directed synthesis of hierarchically mesoporous carbon and its utilization for ciprofloxacin antibiotic remediation. *J. Environ. Chem. Eng.* **2019**, *7*, 102881. [CrossRef]

15. Nguyen, T.-T.; Bui, X.-T.; Luu, V.-P.; Nguyen, P.-D.; Guo, W.; Ngo, H.-H. Removal of antibiotics in sponge membrane bioreactors treating hospital wastewater: Comparison between hollow fiber and flat sheet membrane systems. *Bioresour. Technol.* **2017**, *240*, 42–49. [CrossRef]

16. Wajahat, R.; Yasar, A.; Khan, A.M.; Tabinda, A.B.; Bhatti, S.G. Ozonation and Photo-Driven Oxidation of Ciprofloxacin in Pharmaceutical Wastewater: Degradation Kinetics and Energy Requirements. *Pol. J. Environ. Stud.* **2019**, *28*, 1933–1938. [CrossRef]

17. Tasca, A.L.; Clematis, D.; Stefanelli, E.; Panizza, M.; Puccini, M. Ciprofloxacin removal: BDD anode coupled with solid polymer electrolyte and ultrasound irradiation. *J. Water Process. Eng.* **2020**, *33*, 101074. [CrossRef]

18. Mohd Adnan, M.A.; Julkapli, N.M.; Amir, M.N.I.; Maamor, A. Effect on different TiO$_2$ photocatalyst supports on photodecolorization of synthetic dyes: A review. *Int. J. Environ. Sci. Technol.* **2018**, *16*, 547–566. [CrossRef]

19. Rehman, S.; Ullah, R.; Butt, A.; Gohar, N. Strategies of making TiO$_2$ and ZnO visible light active. *J. Hazard. Mater.* **2009**, *170*, 560–569. [CrossRef]

20. Padervand, M.; Ghasemi, S.; Hajiahmadi, S.; Rhimi, B.; Nejad, Z.G.; Karima, S.; Shahsavari, Z.; Wang, C. Multifunctional Ag/AgCl/ZnTiO3 structures as highly efficient photocatalysts for the removal of nitrophenols, CO$_2$ photoreduction, biomedical waste treatment, and bacteria inactivation. *Appl. Catal. A Gen.* **2022**, *643*, 118794. [CrossRef]

21. Wang, H.; Lewis, J.P. Second-generation photocatalytic materials: Anion-doped TiO$_2$. *J. Phys. Condens. Matter* **2005**, *18*, 421–434. [CrossRef]

22. Padervand, M.; Rhimi, B.; Wang, C. One-pot synthesis of novel ternary Fe$_3$N/Fe$_2$O$_3$/C$_3$N$_4$ photocatalyst for efficient removal of rhodamine B and CO$_2$ reduction. *J. Alloy. Compd.* **2021**, *852*, 156955. [CrossRef]

23. Tan, Y.N.; Wong, C.L.; Mohamed, A.R. An Overview on the Photocatalytic Activity of Nano-Doped-TiO$_2$ in the Degradation of Organic Pollutants. *ISRN Mater. Sci.* **2011**, *2011*, 261219. [CrossRef]

24. Bibi, S.; Ahmad, A.; Anjum, M.A.R.; Haleem, A.; Siddiq, M.; Shah, S.S.; Al Kahtani, A. Photocatalytic degradation of malachite green and methylene blue over reduced graphene oxide (rGO) based metal oxides (rGO-Fe$_3$O$_4$/TiO$_2$) nanocomposite under UV-visible light irradiation. *J. Environ. Chem. Eng.* **2021**, *9*, 105580. [CrossRef]

25. Xiang, Q.; Yu, J.; Jaroniec, M. Nitrogen and sulfur co-doped TiO$_2$ nanosheets with exposed {001} facets: Synthesis, characterization and visible-light photocatalytic activity. *Phys. Chem. Chem. Phys.* **2011**, *13*, 4853–4861. [CrossRef]

26. Mozia, S.; Darowna, D.; Przepiórski, J.; Morawski, A.W. Evaluation of Performance of Hybrid Photolysis-DCMD and Photocatalysis-DCMD Systems Utilizing UV-C Radiation for Removal of Diclofenac Sodium Salt From Water. *Pol. J. Chem. Technol.* **2013**, *15*, 51–60. [CrossRef]

27. Hoffmann, M.R.; Martin, S.T.; Choi, W.; Bahnemann, D.W. Environmental Applications of Semiconductor Photocatalysis. *Chem. Rev.* **1995**, *95*, 69–96. [CrossRef]

28. Gad-Allah, T.A.; Ali, M.E.; Badawy, M.I. Photocatalytic oxidation of ciprofloxacin under simulated sunlight. *J. Hazard. Mater.* **2011**, *186*, 751–755. [CrossRef]

29. Durán-Álvarez, J.C.; Avella, E.; Ramírez-Zamora, R.M.; Zanella, R. Photocatalytic degradation of ciprofloxacin using mono-(Au, Ag and Cu) and bi-(Au–Ag and Au–Cu) metallic nanoparticles supported on TiO$_2$ under UV-C and simulated sunlight. *Catal. Today* **2016**, *266*, 175–187. [CrossRef]

30. Zheng, X.; Xu, S.; Wang, Y.; Sun, X.; Gao, Y.; Gao, B. Enhanced degradation of ciprofloxacin by graphitized mesoporous carbon (GMC)-TiO$_2$ nanocomposite: Strong synergy of adsorption-photocatalysis and antibiotics degradation mechanism. *J. Colloid Interface Sci.* **2018**, *527*, 202–213. [CrossRef]

31. Malakootian, M.; Nasiri, A.; Amiri Gharaghani, M. Photocatalytic degradation of ciprofloxacin antibiotic by TiO$_2$ nanoparticles immobilized on a glass plate. *Chem. Eng. Commun.* **2019**, *207*, 56–72. [CrossRef]

32. Nguyen, L.T.; Nguyen, H.T.; Pham, T.D.; Tran, T.D.; Chu, H.T.; Dang, H.T.; Nguyen, V.-H.; Nguyen, K.M.; Pham, T.T.; Van der Bruggen, B. UV–Visible Light Driven Photocatalytic Degradation of Ciprofloxacin by N,S Co-doped TiO$_2$: The Effect of Operational Parameters. *Top. Catal.* **2020**, *63*, 985–995. [CrossRef]

33. Manasa, M.; Chandewar, P.R.; Mahalingam, H. Photocatalytic degradation of ciprofloxacin & norfloxacin and disinfection studies under solar light using boron & cerium doped TiO$_2$ catalysts synthesized by green EDTA-citrate method. *Catal. Today* **2021**, *375*, 522–536. [CrossRef]
34. Wafi, A.; Szabó-Bárdos, E.; Horváth, O.; Makó, É.; Jakab, M.; Zsirka, B. Coumarin-based quantification of hydroxyl radicals and other reactive species generated on excited nitrogen-doped TiO$_2$. *J. Photochem. Photobiol. A Chem.* **2021**, *404*, 112913. [CrossRef]
35. Mozia, S.; Tomaszewska, M.; Morawski, A.W. Photodegradation of azo dye Acid Red 18 in a quartz labyrinth flow reactor with immobilized TiO$_2$ bed. *Dye. Pigment.* **2007**, *75*, 60–66. [CrossRef]
36. Kamalakkannan, J.; Chandraboss, V.L.; Prabha, S.; Senthilvelan, S. Activated Carbon Loaded N, S Co-Doped TiO$_2$ Nanomaterial and its Dye Wastewater Treatment. *Int. Lett. Chem. Phys. Astron.* **2015**, *47*, 147–164. [CrossRef]
37. Noophum, B.; Sikong, L.; Kooptanond, K. Photocatalytic properties of nitrogen-sulfur co-doped TiO$_2$ films coated on glass fiber. *Adv. Mater. Res.* **2013**, *781–784*, 2237–2240. [CrossRef]
38. Wang, H.; Yang, X.; Xiong, W.; Zhang, Z. Photocatalytic reduction of nitroarenes to azo compounds over N-doped TiO$_2$: Relationship between catalysts and chemical reactivity. *Res. Chem. Intermed.* **2013**, *41*, 3981–3997. [CrossRef]
39. Brindha, A.; Sivakumar, T. Visible active N, S co-doped TiO$_2$/graphene photocatalysts for the degradation of hazardous dyes. *J. Photochem. Photobiol. A Chem.* **2017**, *340*, 146–156. [CrossRef]
40. Mozia, S.; Morawski, A.W. The performance of a hybrid photocatalysis–MD system for the treatment of tap water contaminated with ibuprofen. *Catal. Today* **2012**, *193*, 213–220. [CrossRef]
41. Soares, S.F.; Nogueira, J.; Trindade, T.; Daniel-da-Silva, A.L. Towards efficient ciprofloxacin adsorption using magnetic hybrid nanoparticles prepared with κ-, ι-, and λ-carrageenan. *J. Nanostructure Chem.* **2022**. [CrossRef]
42. Abid, M.F.; Hamza, N.H. Removal of Methyl Violet Dye from Synthetic Wastewater Using a Hybrid Detoxification Process. *Eng. Technol. J.* **2014**, *32*, 1544–1561.
43. Plakas, K.V.; Sarasidis, V.C.; Patsios, S.I.; Lambropoulou, D.A.; Karabelas, A.J. Novel pilot scale continuous photocatalytic membrane reactor for removal of organic micropollutants from water. *Chem. Eng. J.* **2016**, *304*, 335–343. [CrossRef]
44. Serna-Galvis, E.A.; Giraldo-Aguirre, A.L.; Silva-Agredo, J.; Flórez-Acosta, O.A.; Torres-Palma, R.A. Removal of antibiotic cloxacillin by means of electrochemical oxidation, TiO$_2$ photocatalysis, and photo-Fenton processes: Analysis of degradation pathways and effect of the water matrix on the elimination of antimicrobial activity. *Environ. Sci. Pollut. Res.* **2017**, *24*, 6339–6352. [CrossRef] [PubMed]
45. Nakarmi, K.J.; Daneshvar, E.; Eshaq, G.; Puro, L.; Maiti, A.; Nidheesh, P.; Wang, H.; Bhatnagar, A. Synthesis of biochar from iron-free and iron-containing microalgal biomass for the removal of pharmaceuticals from water. *Environ. Res.* **2022**, *214*, 114041. [CrossRef] [PubMed]
46. Xia, S.-M.; Zhang, Y.-Q.; Zheng, Y.-F.; Xu, C.-S.; Liu, G.-M. Enhanced visible light photocatalytic activity of N, F-codoped TiO$_2$ powders with high thermal stability. *Environ. Technol.* **2018**, *40*, 1418–1424. [CrossRef] [PubMed]
47. Chen, F.; Yang, Q.; Yao, F.; Wang, S.; Sun, J.; An, H.; Yi, K.; Wang, Y.; Zhou, Y.; Wang, L.; et al. Visible-light photocatalytic degradation of multiple antibiotics by AgI nanoparticle-sensitized Bi$_5$O$_7$I microspheres: Enhanced interfacial charge transfer based on Z-scheme heterojunctions. *J. Catal.* **2017**, *352*, 160–170. [CrossRef]
48. Xue, Z.; Wang, T.; Chen, B.; Malkoske, T.; Yu, S.; Tang, Y. Degradation of Tetracycline with BiFeO$_3$ Prepared by a Simple Hydrothermal Method. *Materials* **2015**, *8*, 6360–6378. [CrossRef]
49. Jiang, W.-T.; Chang, P.-H.; Wang, Y.-S.; Tsai, Y.; Jean, J.-S.; Li, Z.; Krukowski, K. Removal of ciprofloxacin from water by birnessite. *J. Hazard. Mater.* **2013**, *250–251*, 362–369. [CrossRef]
50. Yu, X.; Kou, S.; Zhang, J.; Tang, X.; Yang, Q.; Yao, B. Preparation and characterization of Cu$_2$O nano-particles and their photocatalytic degradation of fluroxypyr. *Environ. Technol.* **2018**, *39*, 2967–2976. [CrossRef]
51. Zhou, F.; Yan, C.; Liang, T.; Sun, Q.; Wang, H. Photocatalytic degradation of orange G using sepiolite-TiO$_2$ nanocomposites: Optimization of physicochemical parameters and kinetics studies. *Chem. Eng. Sci.* **2018**, *183*, 231–239. [CrossRef]